

Non-rectangular Sampling Topologies for Fast Joint Digital-optical System Optimization

Kathrin Berkner and M. Dirk Robinson

Ricoh Innovations, 2882 Sand Hill Rd, Suite 115
Menlo Park, CA 94025-7054
{berkner,dirkr}@rii.ricoh.com

Abstract: Approximation errors of the MSE merit function for joint digital-optical system optimization are caused by use of rectangular sampling grids. We overcome this problem by adapting the MSE calculations to use flexible non-rectangular sampling topologies.

© 2009 Optical Society of America

OCIS codes: (110.1758) Computational Imaging, (000.4430) Numerical Approximation and Analysis, (070.0070) Fourier Optics and Signal Processing.

1. Introduction

Following the trend pioneered by [1] of designing electro-optical image system by exploring cooperative interaction between optical, detector, and digital processing subsystems, new methods for jointly optimizing both the optical and the digital subsystems based on the linearity of the corresponding filter subsystems have been proposed recently [2]. Therein, the performance of a digital-optical system including Wiener filter restoration is evaluated by propagating the object source information through the complete digital-optical imaging system in two steps. (a) The optical transfer function (OTF) H is computed as

$$H(\omega_1, \omega_2) = \mathcal{F}[|\mathcal{F}(P(r, \phi))|^2], \quad (1)$$

where \mathcal{F} is the Fourier transform operator and $P(r, \phi) = A(r, \phi) \exp(iW(r, \phi))$ is the pupil function with transmission function A and wave front error function W , which measures the optical path difference (OPD) [3]. (b) Image quality after Wiener filtering is predicted by computing the error power spectral density S_e for normalized frequencies $\omega \in [0, 1]$ and integrating over frequencies smaller than the cut-off frequency u of the sensor to obtain the MSE error

$$\text{MSE}(u) = \frac{1}{2\pi} \int_{|\omega_1| < u} \int_{|\omega_2| < u} S_e(\omega_1, \omega_2) d\omega_1 d\omega_2, \quad S_e(\omega_1, \omega_2) = \frac{S_{uu}(\omega_1, \omega_2) S_{nn}(\omega_1, \omega_2)}{|\mathcal{H}(\omega_1, \omega_2)|^2 S_{uu}(\omega_1, \omega_2) + S_{nn}(\omega_1, \omega_2)}, \quad (2)$$

where S_{uu} is the power spectral density of the source, S_{nn} the noise power spectral density, and $u \in [0, 1]$. Using MSE as the merit function in the optimization step of a digital-optical imaging system design has led to novel system designs and functionalities, e.g. the one proposed in [4].

Implementing the MSE function in software requires performing a discretization of the OPD and S_e domains. The discretization used in the current implementation to create the results in [2, 4] consists of the following steps. (1) Compute OPD values at pupil locations intersecting a regular square grid of size $B \times B$ by ray tracing using Zemax software [5]. A typical value for B is 64. (2) Compute pupil function samples on a regular square grid of size $B \times B$. (3) Apply FFTs to pupil function values to obtain the OTF H on a $2B \times 2B$ grid (Eq. 1). (4) Compute S_e values on $2B \times 2B$ grid (Eq. 2). (5) Compute MSE by integration of S_e values on grid $2B \cdot u \times 2B \cdot u$ to include only samples inside the cut-off-frequency of the sensor (Eq. 2). Integration is performed by applying the rectangle rule. Whereas this implementation supported a break-through in the design of jointly-designed digital-optical systems two major problems have been noticed. One problem is that accuracy of the MSE measure suffers when the sensor's cut-off frequency is low, i.e. when the number of samples on the restricted S_e grid of size $2B \cdot u \times 2B \cdot u$ is small. The resulting MSE approximation error causes calculation of design solutions that seem to be trapped in local minimal away from the optimal solution. This problem can be solved by increasing the sampling frequency of S_e which means to increase B and, therefore, the number of rays traced through the optical system. The second problem is that the implementation for large B becomes very slow, due to computationally expensive ray tracing. Solving the second problem has been attempted in [6] by computing the OTF from a finite Taylor-series expansion of the pupil function without showing acceptable speed-up for largely aberrated systems.

In this paper, we introduce a new architecture for computing the MSE that eliminates the problems of the current implementation by enabling the use of non-rectangular grid topologies with fewer samples in the OPD and S_e domains.

The propagation of information from one domain to another is performed using computationally inexpensive interpolation techniques and the Nonequispaced FFT (NFFT) [7], a modified FFT applicable to compute Fourier transform coefficients at nonequispaced frequency locations. Integration over S_e to obtain the MSE measure is approximated by applying a Gauss-quadrature integration method. An overview of the proposed new pipeline architecture is shown in Fig. 1, and details will be explained in the following. For an example design space we demonstrate the advantages of the new architecture in terms of computational complexity and accuracy control compared to the current architecture.

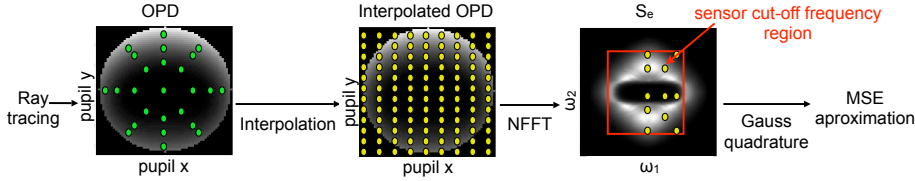


Fig. 1. Proposed novel pipeline architecture for computing the MSE measure for optimization of digital-optical imaging systems.

2. New MSE pipeline with non-rectangular sampling grids

Since ray tracing to pupil locations intersecting a dense grid of size $B \times B$ with $B \geq 64$ has been identified as the main reason for the slow performance of the current MSE calculation one goal is to reduce the number of OPD values obtained via ray tracing by changing the sampling grid topology to one that is more suitable for capturing OPD information while still maintaining good system accuracy. In order to achieve that goal we apply a concept already used to calculate merit functions for purely optical systems, namely sampling the OPD values on a polar grid of L rings and K arms [8, 5]. The polar grid sampling strategy has been shown appropriate for efficiently sampling the OPD on the pupil, since the OPD is typically represented by a few lower order Seidel aberrations, which are modeled as polynomials in radius and angle. In our proposed pipeline we compute samples on a regular $B \times B$ grid by linearly interpolating the OPD samples obtained via ray tracing on a polar grid to the rectangular grid in order to have appropriated samples for performing the required Fourier transform operations (see Eq. 1).

To improve the accuracy of the integration of the the Wiener filter error estimate S_e we apply a Gaussian quadrature integration method. This method evaluates an integrand function f at given locations (nodes), that are independent of the integrand itself, and approximates the integral by a weighted sum of the integrand values at those nodes, i.e. $\int_{-1}^1 f(x)dx \approx \sum_{k=1}^p w_k f(x_k)$. The nodes x_k for a Gauss quadrature are zeros of Legendre polynomials and the weights w_k are related to those polynomials [9]. The order of the quadrature, p , depends on the desired accuracy of the approximation and the smoothness of the integrand f . Using a Gauss quadrature for approximation of the MSE results in $MSE(u) \approx \sum_j \sum_k v_{j,k} S_e(\omega_{1,j}, \omega_{2,k})$ with weights $v_{j,k}$ and sampling locations $\omega_{1,j}, \omega_{2,k}$ in the interval $[0, u]$, where the sampling locations are the quadrature nodes normalized to fit the interval $[0, u]$. Sampling the half-plane $[-0, u]^2$ only is sufficient due to symmetry of S_e . Since Gauss quadrature nodes are not located on a regular rectangular grid we use the Nonequispaced FFT (NFFT) [7] to compute S_e values at quadrature nodes. Gauss quadratures are used in purely optical design when approximating the OPD-RMS merit function from OPD values sampled on a polar grid [8, 5]. In that case no FFT operations are required since the diffraction integral does not need to be computed.

3. Experiments

In order to test accuracy of the proposed pupil sampling followed by interpolation and MSE calculation using a Gaussian quadrature we consider the design space of a singlet with fixed lens at $F \# = 4.6$ and BK7 glass. The optical design space is composed of thickness and bending, allowing the thickness of the lens to vary between 0 and 3mm and the curvature of the second surface to vary between -0.1 to 0.1 inverse mm.

OPD values on a 64×64 square grid via ray tracing as created by the current implementation serve as ground truth data. To evaluate the new architecture, OPD values on the same 64×64 grid are approximated by first obtaining OPD values on a polar grid with L rings and K arms via ray tracing and then interpolating those values to the 64×64 square grid using linear interpolation. Whereas the arms are at equally spaced locations, the rings are located at $\sqrt{\frac{\ell}{L}}, \ell = 1, \dots, L - 1$ [8, 10]. The difference between the interpolated and the ground truth data is computed as an L_2 error, integrated over the entire design space. The results for $L = 1, \dots, 10, K = 4, 8, \dots, 40$, are shown in Fig. 2. Given a threshold of 0.1λ used traditionally for OPD-RMS to assure appropriate quality of a purely optical system,

we conclude that sampling the polar grid at 240 locations (10 rings and 24 arms) followed by linear interpolation is sufficient to provide appropriate OPD accuracy. Reducing the numbers of rays to be traced from 3557 in the current to 240 in the proposed new implementation leads to significant speed up of the pupil function approximation by a factor of 15.

The accuracy of integration of S_e is analyzed using different numerical integration techniques. In the current implementation first 128^2 S_e samples have to be computed. Then a simple rectangle rule is applied to $(128 \cdot u)^2$ samples having a fixed grid spacing independent of u . That implies that for small u only very few samples are included in the integration. Two integration methods using different non-rectangular grid topologies are considered: (a) performing a Gauss quadrature integration in both dimensions of the integral, and (b) performing a Gauss quadrature in the radial and a trapezoidal-rule integration method in the angular dimension. The number of integration nodes for all methods varies between $p = 4$ and 64 for one quadrant in the S_e plane. For $u = 0.2$, the MSE is calculated for different defocus locations -2.75 , and -6.0 , where -2.75 is close to and -6.0 far away from the optimal defocus location in the considered design space. The computed MSE values are shown in Fig. 2 and demonstrate that at defocus location away from the optimal location the equispaced rectangular and trapezoidal methods show unstable behavior for small number of nodes. In comparison, the quadrature-based methods show a more stable behavior. This observation explains the accuracy problems occurring with the current implementation at small u -values implying an under-sampling of the relevant S_e region. Close to the optimal defocus location all methods perform similarly. We conclude that a quadrature of order $p = 16$, resulting in $2p^2 = 512$ S_e -samples for two quadrants, provides acceptable MSE accuracy. For comparison, in the current implementation, 128^2 S_e -samples on an equispaced grid need to be computed.

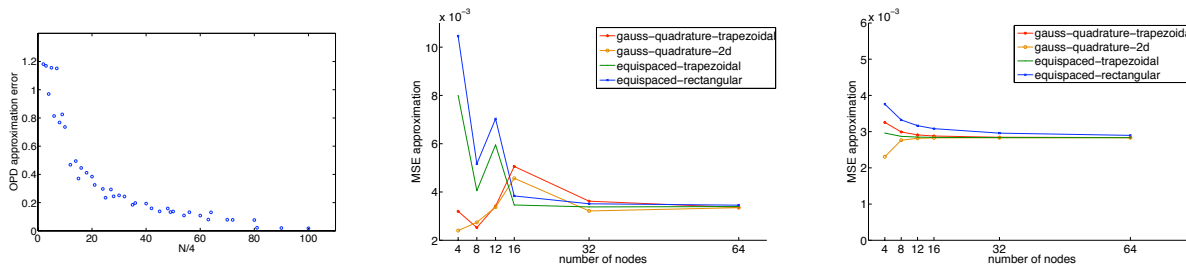


Fig. 2. Accuracy of proposed MSE calculation: OPD accuracy after interpolation from a polar grid with $N = K \times L$ samples to a 64×64 regular grid (left). Integration accuracy over S_e for different integration methods and two different defocus locations -6.0 (middle) and -2.75 (right).

4. Conclusions

We have introduced a new architecture computing the MSE merit function used in optimization of joint digital-optical imaging systems. The new architecture overcomes the accuracy and complexity problems of the current implementation by including non-rectangular sampling grids for the OPD and Wiener filter error estimator domains and NFFT operations to propagate information between those domains.

References

1. Edward R. Dowski and W. Thomas Cathey, "Extended depth of field through wave-front coding," *Applied Optics*, vol. 34, no. 11, pp. 1859–1866, 1995.
2. David Stork, M. Dirk Robinson, "Theoretical Foundations for joint digital-optical analysis of electro-optical imaging systems," *Applied Optics*, vol. 47, no. 10, pp. B64–B75, 2008.
3. J.W. Goodman, *Introduction to Fourier Optics*, McGraw-Hill, New York, 1986.
4. M. Dirk Robinson and David Stork, "Joint digital-optical design of imaging systems for grayscale objects," in *Proceedings of the SPIE European Optical Design Conference*, Sept. 2008.
5. Z. D. Corporation, "ZEMAX User's Guide," 2004.
6. Saeed Bagheri, Daniela Pucci de Farias, and George Barbastathis, "Reduced-complexity representation of the coherent point-spread function in the presence of aberrations and arbitrarily large defocus," *Journal of the Optical Society of America*, vol. 23, no. 10, pp. 2476–2493, 2006.
7. Daniel Potts, Gabriele Steidl, Manfred Tasche, "Fast Fourier transforms for nonequispaced data: A tutorial," *Modern Sampling Theory: Mathematics and Applications*, pp. 249–274, 2001.
8. G. W. Forbes, "Optical system assessment for design: numerical ray tracing in the Gaussian pupil," *J. Opt. Soc. Am.*, vol. 5, no. 11, pp. 1943–1956, 1988.
9. W. Press, S. A. Teukolsky, W. T. Vetterling, B.P. Flannery, *Numerical Recipes*, Cambridge University Press, 2007.
10. H.H. Hopkins, M.J. Yzuel, "The Computation of Diffraction Patterns in the Presence of Aberrations," *Journal of Modern Optics*, vol. 17, no. 3, pp. 157–182, 1970.